Isotope effects on the photodesorption processes of X2O (X = H,D) and HOD ice

J. Koning, G. J. Kroes, and C. Arasa

Citation: The Journal of Chemical Physics **138**, 104701 (2013); doi: 10.1063/1.4793733
View online: http://dx.doi.org/10.1063/1.4793733
View Table of Contents: http://scitation.aip.org/content/aip/journal/jcp/138/10?ver=pdfcov
Published by the AIP Publishing

Isotope effects on the photodesorption processes of X_2O (X = H,D) and HOD ice

J. Koning, G. J. Kroes, and C. Arasa
Gorlaeus Laboratories, Leiden Institute of Chemistry, Leiden University, P. O. Box 9502, 2300 RA Leiden, The Netherlands

(Received 17 December 2012; accepted 14 February 2013; published online 8 March 2013)

To investigate the isotope effects on the photodesorption processes of X_2O (X = H,D) ice, molecular dynamics calculations have been performed on the ultraviolet photodissociation of an H_2O or a D_2O molecule in an H_2O or a D_2O amorphous ice surface, and on HOD photodissociation in an H_2O amorphous ice surface, where the photodissociated molecules were located in the top four or five monolayers at ice temperatures of 10, 20, 30, 60, and 90 K. Three photodesorption processes can occur upon X_2O photodissociation: X atom photodesorption, OX radical photodesorption, and X_2O (or HOD) molecule photodesorption. X_2O (or HOD) photodesorption can occur after recombination of X and OX, or after an energetic X atom photofragment kicks a surrounding X_2O molecule from the ice surface. Isotope effects are observed for the X atom and the OX radical photodesorption as well as for the kick-out photodesorption. However, no isotope effects were noticeable for the photodesorption of recombined X_2O molecules. The average D atom photodesorption probabilities are about a factor 0.9 smaller than those for the H atom, regardless of the isotope of the surrounding ice system. Also, the kick-out mechanism is more likely to occur if a D photofragment is created upon dissociation than if an H atom is created. These observations can be explained by more efficient energy transfer from the D atom to water molecules than from the H atom. Reasoning based on the X_2O phonon frequencies associated with the librational modes and energy transfer efficiencies explain why the OX radical photodesorption probabilities are noticeably larger if the OX radical desorbs from a D_2O ice system than from an H_2O ice system. Also, the OX radical photodesorption is more probable upon dissociation of DOX (X = H,D) than upon dissociation of HOX (X = H,D), because the initial kinetic energy of the OX radical is larger if the dissociation products are D + OX than H + OX. The branching ratio of $\frac{OD}{OH}$ desorption following photodissociation of an HOD molecule in ice (about 1.0) is much lower than the $\frac{OD}{OH}$ branching ratio in gas-phase HOD photodissociation. This may lead to differences in isotope fractionation in OH(g) formation in dense and diffuse clouds in the interstellar medium. © *2013 American Institute of Physics*. [http://dx.doi.org/10.1063/1.4793733]

I. INTRODUCTION

In the interstellar medium (ISM), sub-micron sized dust particles are covered with icy mantles. The ice mainly consists of H_2O and of other organic molecules, such as CO, CH_3O, and NH_3, among others.[1,2]

The abundance of gaseous water in the ISM cannot be explained by merely gaseous formation or thermal desorption of H_2O from ice surfaces.[3–5] A non-thermal desorption mechanism which could explain the observed abundance of gaseous water in the ISM is initiated by ultraviolet (UV) photolysis.[3,6] Irradiation of UV photons can photo-excite the water molecules present in ice mantles and cause dissociation into H and OH, which can lead to photodesorption of the fragments or desorption of the recombined H_2O molecule. H_2O can also desorb from ice through the kick of an energetic H atom that transfers its momentum to a surrounding water molecule.[6–8]

Atomic hydrogen and OH radicals formed upon dissociation of H_2O can travel in the ice and react with small organic molecules (e.g., CO),[9] and these reactions may lead to the formation of more complex organic molecules (e.g., CH_3CHO). The abundance of heavy radicals, such as HCO and CH_3O, in the icy mantles is predominantly a result of H_2O photodissociation.[10,11] UV photon fluxes are estimated to be 1 photon per dust particle per day.[12] Thus, one single photon excitation process of H_2O is likely to be completed before the next photon arrives at the ice surface.

Isotope effects regarding the photo-chemistry of H_2O have been studied theoretically[12–16] and experimentally.[3,17–20] Absorption cross sections of gas-phase H_2O,[14,15,21] D_2O,[14,15] and HOD[13,15,16] have been calculated for the rovibrational ground state and for rovibrationally excited states, and have also been measured experimentally for gas-phase H_2O,[18–20] D_2O,[18,19] and HOD.[18,22] Moreover, in other experiments the photon-induced[22] dissociation and ion-induced[23] dissociation processes of gas-phase HOD have been studied, and the branching ratios, which depend on laser frequency,[16,22,24] have been provided. Zhang *et al.*[16] and Engel *et al.*[13] both predicted that the $\frac{H+OD}{D+OH}$ ratio is about 2.5 at the maximum of the absorption spectrum. Photodissociation of both H_2O[6,7,25,26] and D_2O molecules[12] in H_2O and D_2O ice, respectively, have been studied theoretically using Molecular Dynamics (MD) calculations at different ice temperatures.

There are also laboratory experiments regarding UV photodissociation of H_2O and D_2O ice where the ice sample is irradiated by multi-photon sources at excitation energies close to the Ly-α value.[3,27–29] Therefore, in these experiments X_2O (X = H,D) molecules could be excited to higher electronic states, which allows the formation and consequently the desorption of species such as X_2, O_2, and X_2O_2. However, in the previous MD simulations,[6,7,12,25,26] only excitation to the first electronically excited state was considered.

In a different kind of experiment, Hundt *et al.*[30] measured the sticking probabilities of D_2O molecules on X_2O ice, using a molecular beam with an average translational energy of 38 kJ/mol and 69 kJ/mol at an ice temperature of 108 K. They concluded that the sticking probabilities are near unity, and larger for D_2O on D_2O ice than on H_2O ice, due to isotope effects. Similar sticking probabilities were observed by Batista *et al.*[31] for the sticking of H_2O on crystalline H_2O ice at 20 K using low energy (48 kJ/mol) H_2O molecular beams. High sticking probabilities of H_2O on ice complicate the desorption measurements of H_2O in photodesorption experiments due to the freeze-out of H_2O in the used vacuum chambers.

In this paper, we will report MD calculations on the photodissociation of an X_2O^* molecule—the * indicates that the molecule is in the first electronically excited state—in a X_2O amorphous ice system in order to investigate isotope effects on the photodesorption processes. In particular, MD simulations have been carried out for H_2O^* in H_2O and D_2O amorphous ice, and also for D_2O^* in H_2O and D_2O amorphous ice at T_{ice} = 10, 20, 30, 60, and 90 K. Some of these results were taken from previous MD simulations by Arasa *et al.*[12] Also, MD simulations for HOD* in an H_2O amorphous ice system have been performed.

This paper is set up as follows. In Sec. II the method for the MD calculations is described, in Sec. III the results are shown, and in Sec. IV the conclusions are presented.

II. METHOD

MD calculations were carried out to investigate the isotope effects on the photodesorption processes of an X_2O ice system. A description of the potentials that were used during the dynamics is given in Sec. II A, and a description of the ice system is given in Sec. II B. Finally, details on the dynamics method are provided in Sec. II C.

A. Potentials

In order to carry out the MD calculations, a good description of all the interactions is necessary. In particular, we have used analytical pair potentials and the total Potential Energy Surface (PES) can be written as

$$V_{tot} = V_{ice} + V_{X_2O^*\text{-ice}} + V_{X_2O^*}. \quad (1)$$

The first term of Eq. (1) describes the intermolecular interactions between the X_2O molecules inside the ice, excluding the excited molecule. This term consists of H_2O–H_2O interactions described by the TIP4P potential,[32] and all the molecules are kept rigid.

The second term of Eq. (1), $V_{X_2O^*-ice}$, accounts for the interactions between the excited X_2O molecule, which is fully flexible, and the other water molecules, as well as the interactions between the photofragments and the molecules. This term consists of three potentials: $V_{H_2O^*-H_2O}$, V_{H-H_2O}, and V_{OH-H_2O}. Before the excited molecule is dissociated, the interaction of the excited X_2O molecule with the ice is given by $V_{H_2O^*-H_2O}$, which is described by an adjusted TIP3P potential.[32] After dissociation of X_2O, the interactions of the photofragments with the ice are given by V_{H-H_2O} and V_{OH-H_2O}, which represent the X atom interactions with the water molecules and the OX radical interactions with the water molecules according to the H–H_2O PES and to the OH–H_2O PES,[6] respectively. Switching functions are used to change smoothly from $V_{H_2O^*-H_2O}$ to V_{H-H_2O} and V_{OH-H_2O} while the dissociation proceeds.[6,7]

The third term, $V_{X_2O^*}$, represents the intramolecular interactions in the excited X_2O molecule, and is given by the gas-phase H_2O Dobbyn-Knowles (DK) PES.[15,33,34] For the dynamics of D_2O and HOD photodissociation the same PESs were used, but with appropriate masses in each case. All the potentials and the corresponding switching functions used in this study are the same as the ones used for H_2O and D_2O ice photodissociation calculations. Details on these potentials and the switching functions between the potentials can be found in Refs. 6 and 26.

B. Description of amorphous ice

The H_2O and D_2O amorphous ice systems have been set up at T_{ice}= 10, 20, 30, 60, and 90 K using the same procedures as those used in our previous studies.[6,7,12,25,26] For more details we refer to Refs. 6, 7, 25, and 26.

C. Dynamics

For each molecule in the top four monolayers (MLs) of the ice, 200 different initial configurations were generated for the dynamics calculations. Six photodissociation scenarios have been considered at T_{ice} = 10, 20, 30 , 60, and 90 K:

1. H_2O^* dissociation in an H_2O amorphous ice (H_2O^*/H_2O).
2. H_2O^* dissociation in a D_2O amorphous ice (H_2O^*/D_2O).
3. D_2O^* dissociation in an H_2O amorphous ice (D_2O^*/H_2O).
4. D_2O^* dissociation in a D_2O amorphous ice (D_2O^*/D_2O).
5. HOD* dissociation into H + OD in an H_2O amorphous ice (HOD*/H_2O).
6. HOD* dissociation into D + OH in an H_2O amorphous ice (DOH*/H_2O).

For each of the studied scenarios the appropriate masses of the photo-excited molecule and the other molecules in the ice have been taken into account.

To initialize the trajectories, a Wigner phase-space distribution function is fitted to the ground-state vibrational wavefunction of gas-phase H_2O.[35] A Monte Carlo procedure is used to sample the initial positions and momenta of the atoms of the selected molecule. Then, the molecule is brought to the first electronically excited state on the DK PES[15,33,34] via a vertical excitation. The Wigner distribution of gas-phase D_2O has the same functional form as the Wigner distribution of gas-phase H_2O, but the α values from Eq. (5.20) in Ref. 35 are corrected with $\sqrt{2}$, such that $\alpha_{i,\,D_2O} = \sqrt{2}\alpha_{i,\,H_2O}$ for $i = r$, R, γ.

The Wigner distribution of gas-phase HOD also has the same functional form as that of gas-phase H_2O, but different α values were computed using Eq. (5.16) in Ref. 35 to account for the different masses as well as the frequencies of the OH stretch, OD stretch, and the bend vibration (Refs. 36–38) of the HOD molecule. The symmetry of the H_2O or D_2O molecule is lost if an HOD molecule is considered, therefore two different Wigner distribution functions can be set up for HOD depending on whether the OH or the OD bond is associated with the Jacobi coordinate r. For reasons of convenience we consistently modeled the dissociation reaction where an ABC molecule dissociates into fragments A and BC. Thus, Wigner distributions were computed for both the "HOD" molecule and the "DOH" molecule. If the dynamics lead to the ABC $\rightarrow$ AB + C dissociation reaction (e.g., HOD $\rightarrow$ OH + D), the trajectory was stopped and not taken into account for the discussion of desorption processes. These trajectories were taken into account to compute the branching ratio of the HOD photodissociation reaction.

Newton's equations of motion are integrated in time using a leapfrog algorithm with a time step of 0.02 fs and a maximum time of 20 ps to simulate the photodissociation dynamics. The outcome channels of the photodissociation dynamics of X_2O (X = H,D) in H_2O or D_2O ice are (1) X atom desorption while the OX radical remains trapped in the ice or on the ice surface, (2) OX radical desorption while the X atom remains trapped in the ice or on the ice surface, (3) X atom and OX radical desorption, (4) trapping of both the X atom and the OX radical, (5) recombination of the X atom and the OX radical to form X_2O which desorbs or (6) remains trapped. The outcome channels for the dissociation dynamics of HOD in H_2O ice are the same as for the dissociation dynamics of X_2O in H_2O or D_2O ice, with the remark that the recombination of the X atom and the OX radical lead to formation of HOD instead of X_2O. An outcome channel which may exist independently of the outcome channels 1–6 is the desorption of an X_2O molecule upon a collision with an X atom photofragment. This is called the "kick-out" mechanism. The criteria used to end trajectories are the same as for previous H_2O and D_2O ice photodissociation MD studies.[6,7,12,25,26]

For each X_2O molecule selected to be excited, 200 initial condition were generated to study the photodissociation dynamics in both H_2O and D_2O ices. Since a ML consists of 30 molecules and only excitation of X_2O in the top four MLs is considered, 6000 trajectories are run per ML and 24 000 trajectories are run at each ice temperature per system. However, for every HOD molecule to be photodissociated, 300 initial conditions were generated if the Wigner distribution was set up for dissociation of HOD into H + OD, whereas 700 initial conditions were generated if the Wigner distribution was set up for dissociation of HOD into D + OH, because the branching ratio $\frac{H+OD}{D+OH}$ was calculated (see Fig. 3 in Ref. 13 and Fig. 3 in Ref. 16) to lie between 2 and 3 around the maximum of the absorption spectrum of gas-phase HOD. As a first approximation, we would expect roughly the same value for the branching ratio for the HOD ice photodissociation reaction computed by using MD simulations as for the branching ratio around the maximum of the absorption spectrum. The branching ratio implies that extra initial conditions must be generated to have proper statistics for the photodissociation calculations. The number of initial conditions was chosen such that at least 6000 trajectories were simulated for each ML. At 10 K, 500 initial conditions per molecule were selected for the dissociation dynamics of HOD into photofragments H and OD in H_2O ice, because this number of trajectories was also used to evaluate the absorption spectrum of HOD.

III. RESULTS AND DISCUSSION

In this section we present results regarding the photodesorption events (i.e., X atom (Sec. III A), OX radical (Sec. III B), and X_2O molecule (Sec. III C) photodesorption) that can occur following UV photodissociation of an X_2O^* molecule in X_2O ice at different ice temperatures. In Sec. III D the photodesorption processes of HOD in H_2O ice are discussed.

A. X(=H,D) atom photodesorption

The probabilities of the outcome channels after the photo-excitation of a single water molecule have been calculated for the initially excited molecule being located in the top four MLs of the ice, because previous reports have shown that excitation of these molecules may lead to photodesorption.[6,25] The X(=H,D) atom photodesorption outcome channel is the most important desorption event (more details in Refs. 6, 7, and 26). Due to the weak interaction between X atom and the ice,[10] the X atom may also first accommodate and then desorb through thermal desorption. However, this cannot be described in our calculations due to the limited time scale of our simulations ($t_{max} = 20$ ps).

The photodesorption probability ($p_i = \frac{N_i}{N_{total}}$, $\epsilon_i = \sqrt{\frac{p_i(1-p_i)}{N_{total}}}$, i = photodesorption event, and ϵ_i is the standard error in the probability) of the X atom from an X_2O ice system has been calculated for and averaged over the top four MLs at different ice temperatures, and is plotted in Fig. 1 for the first four dissociation scenarios presented previously in Sec. II C. The desorption of an X atom can be accompanied by either trapping of the OX radical or desorption of the OX radical (outcome channels 1 and 3, respectively), but these processes are not distinguished further here.

The H atom photodesorption probabilities are larger than those for D in the H_2O and D_2O amorphous ice systems (Fig. 1). H atoms desorb more easily than D atoms do: the velocity of the H atom upon H_2O photodissociation is larger than the velocity of the D atom upon D_2O photodissociation,

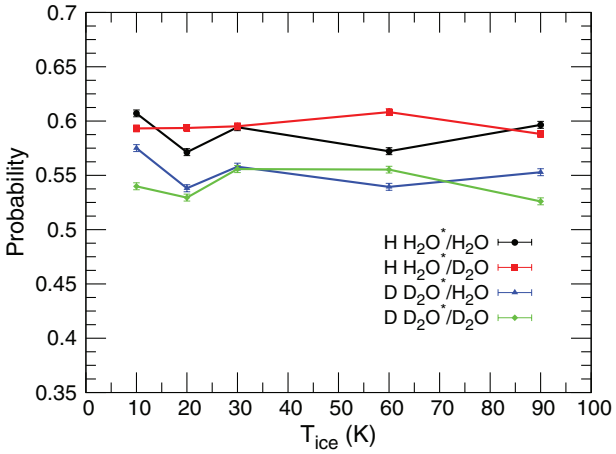

FIG. 1. Photodesorption probabilities of photofragment X following X_2O^* photodissociation in an X_2O ice system (denoted in legend as X X_2O^*/X_2O) averaged over the top four MLs as a function of ice temperatures (T_{ice}).

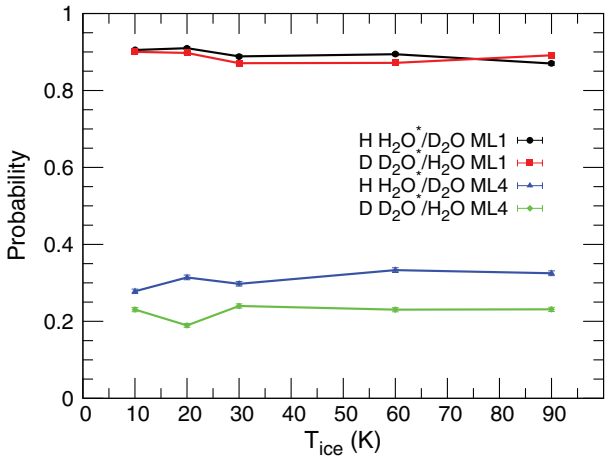

FIG. 2. Photodesorption probabilities for the H atom after H_2O^* photodissociation in a D_2O ice system (H H_2O^*/D_2O) and for the D atom after D_2O^* photodissociation in an H_2O ice system (D D_2O^*/H_2O) for the situation where the photo-excited molecule is initially located in monolayer 1(ML1) and 4(ML4) as a function of T_{ice}.

because the H atom is lighter than the D atom. The H photodesorption probability averaged over the top four MLs and over all ice temperatures is 59.6% if the H_2O molecule is initially excited in a D_2O ice system and 58.8% if the H_2O molecule is initially excited in an H_2O ice system. If a D_2O molecule is dissociated, the averaged probability over the top four MLs and over all the ice temperatures of D desorbing from the ice surface is about 55.3% and 54.1% if excitation occurs in an H_2O and in a D_2O ice system, respectively. This result can also be explained by energy transfer from the X atom to the surrounding water molecules upon collisions. A hard sphere kinematic model for elastic collisions[39,40] states that the energy transfer from the X atom to a water molecule (which is assumed to be stationary initially) is dependent on the mass ratio of the two colliding objects, as follows:

$$r = \frac{4\alpha}{(1+\alpha)^2} \tag{2}$$

with r being the fraction of the energy which is transferred during the collision, and α being the mass ratio of the colliding species. According to Eq. (2), which for our purposes is only used qualitatively, D atoms transfer their energies more easily to the surrounding molecules than H atoms do, since $\alpha_H = \frac{m_H}{m_{X_2O}} < \frac{m_D}{m_{X_2O}} = \alpha_D$. From Fig. 1 it is noticeable that there are no striking differences between H atoms desorbing from H_2O and D_2O ice, and between D atoms desorbing from H_2O and D_2O ice, regarding the photodesorption probabilities for each ice temperature averaged over the top four MLs.

On average, a hydrogen atom desorbs from a D_2O ice system with a probability of about 4.3% higher than a deuterium atom from an H_2O ice system. This arises from differences in the probability of X atoms desorbing from MLs 2–4, as is illustrated in Fig. 2 for ML1 and ML4. If the dissociation occurs in the first ML, H and D atoms will desorb with almost identical probabilities, but there is a clear difference in desorption probabilities if the X_2O molecule is dissociated in ML 4: H atoms desorb from D_2O ice with higher probabilities than D atoms desorb from an H_2O ice system for MLs 2–4.

Since photofragments formed deeper in the ice first have to travel from the bottom to the top of the ice surface to be able to desorb, the difference in the desorption probabilities can be explained by energy transfer in collisions of the photofragments with the molecules in the ice system. In agreement with this picture, the energy of the desorbed X atom is strongly influenced by the location of the initially excited molecule. The average energy of the desorbed H atoms from H_2O molecules dissociated in the first ML of a D_2O system is 2 eV. If the excited molecule is initially located in the fourth ML, the energy of the desorbed H atom is only 1.25 eV. The average energy of a D atom desorbed from an H_2O ice system is 1.56 eV and 0.83 eV if dissociation takes place in the first and fourth ML, respectively.

The average distance traveled at 90 K by an H atom formed if H_2O is dissociated in a D_2O ice system is around 10.1 Å, the one traveled by D atoms formed upon D_2O dissociation in an H_2O ice system is about 7.6 Å, and the ones traveled by H and D atoms formed upon H_2O and D_2O photodissociation are 9.1Å and 8.4 Å, respectively.[12] The distance traveled by an X atom in X_2O ice (d_{X/X_2O}) can be summarized as follows: $d_{D/H_2O} < d_{D/D_2O} < d_{H/H_2O} < d_{H/D_2O}$.

This trend is fully consistent with the efficiency of the energy transfer that is expected on the basis of the mass ratio of the X atom and the stationary water molecules (Eq. (2)). Thus, the less the energy is transferred the larger the distance the X atom can travel in the ice.

The ice temperature does not greatly affect the average energy of the desorbed X atom or the average traveled distance of the X atom if trapping occurs. At the statistical accuracy of our calculations, the ice temperature also has no detectable influence on the X photodesorption probability because the translational energies with which X is formed (≈2.5 eV) following X_2O photodissociation is more than 2 orders of magnitude larger than the thermal translational energies of X_2O between 10 and 90 K, the averages of which are in the range 1.3–12 meV.[26] Therefore, the flow of energy is predominantly from the H-atoms to the X_2O molecules, and the

initial temperature (initial average kinetic energy) of the X_2O molecules is not important. In contrast, the surface temperature has been observed to be highly relevant to experiments on sticking of hydrogen atoms to ice, because in this case the initial kinetic energies of the H atoms and of the X_2O molecules usually are of equal order of magnitude and comparable to the binding energy of H to a H_2O surface. For instance, Al-Halabi *et al.* investigated sticking of H-atoms to ice surfaces for initial H-kinetic energies in the range 100–600 K (9–52 meV) for surface temperatures in the range 10–70 K, corresponding to X_2O molecules with average kinetic energies in the range 1.3–9.0 meV,[41] while the adsorption energy of an H-atom to an ice surface should be less than 30 meV.[42]

B. OX radical photodesorption

The OX radical photodesorption probability is the second most important photodesorption mechanism and is calculated by summing over the probabilities of two channels: the desorption of the OX radical if the X atom remains trapped, and the desorption of both the OX radical and the X atom. The OX photodesorption is also dependent on the initial location of the excited X_2O molecule. In Table I we have summarized the OX radical photodesorption probabilities for the MLs where the excited X_2O molecule is initially located, and it can be seen that the probability of an OX radical desorbing from the ice decreases with increasing depth, especially going from ML2 to ML3. The reason for this trend is that the deeper the initially photodissociated molecule is in the ice surface, the more likely it is that a resulting OX fragment that is moving upwards will encounter a X_2O molecule on its way. Because the mass ratio of OX and X_2O is almost equal to one, such an encounter usually causes OX to lose much of its energy, precluding desorption of OX. In our study the X_2O molecules are binned in monolayers depending on their initial coordinate for motion perpendicular to the surface, and because we model an irregularly shaped, amorphous ice surface, it is possible that molecules assigned to ML2 have no X_2O molecule right above them. However, going deeper into the ice this becomes progressively less likely, which explains the trend observed.

The OH photodesorption probabilities from H_2O ice and the OD photodesorption probabilities from D_2O ice were already calculated earlier[12] for most of the ice temperatures considered. Here, the OH desorption probabilities from D_2O ice and OD desorption probabilities from H_2O ice have also been calculated. In Fig. 3 the photodesorption probabilities of OX averaged over the top four MLs are plotted for each investigated system. The photodesorption probabilities for OD desorbing from D_2O ice are a factor of 2.7 larger than those for OH desorbing from H_2O ice. However, the OH radical photodesorption probabilities from D_2O ice and the OD radical photodesorption probabilities from H_2O ice are very similar. Two effects can be responsible for these observations.

TABLE I. OX photodesorption probabilities for H_2O photodissociation in a D_2O ice system (OH H_2O^*/D_2O) and for D_2O photodissociation in an H_2O ice system (OD D_2O^*/H_2O) per ML for the top four MLs averaged over all ice temperatures.

	OH H_2O^*/D_2O $\times 10^{-3}$	OD D_2O^*/H_2O $\times 10^{-3}$
ML1	49.5	59.0
ML2	32.7	29.4
ML3	1.37	5.79
ML4	0.17	0.04

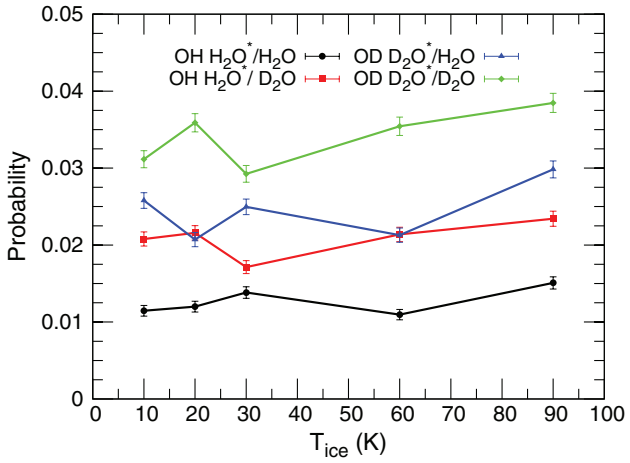

FIG. 3. Photodesorption probability of the OX radical photofragment following X_2O^* photodissociation in an X_2O ice system (denoted in legend as OX X_2O^*/X_2O) averaged over the top four MLs as a function of T_{ice}.

(1) The OD radicals have higher kinetic energies than the OH radicals do upon the initial D_2O and H_2O photodissociation, respectively, making it easier for OD radicals to move through the surface and finally desorb. In the gas-phase, where the X_2O molecule is isolated, conservation of momentum and energy must be obeyed after dissociation; $p_{OX} + p_X = 0$, and $E_{OX} + E_X = \Delta E$, with ΔE being the initial available energy; $\Delta E = E_{exc} - E_{diss}(X_2O)$, which is the difference between the excitation energy and the dissociation energy of X_2O into X + OX. More specifically, the initial kinetic energy of the OX fragments E_{OX} may be estimated from:[12]

$$E_{OX} = \frac{\Delta E}{1 + \frac{m_{OX}}{m_X}}. \quad (3)$$

It is easy to see that, according to Eq. (3), for the same excitation energy E_{exc}, E_{OD} should be about a factor 1.8 larger than E_{OH}, due to the difference in mass ratio. Here, we have not yet considered the role played by the final rotational and vibrational energy of the OX fragment. However, this should not change the conclusions much, for the following two reasons. First, due to a lack of translation-rotation coupling in the exit channel of the A-state water potential, the OX fragment is produced with little rotational energy. At the temperatures here considered, the X_2O molecules will originally be in the ground state for the water bend vibration. Calculations on gas phase water photodissociation predict that under these conditions the rotational energy in the final OX fragment should amount to no more than 35 meV.[43] Second, although much more energy is released in the vibration of the OX fragment, the amounts of the average vibrational energy of the OX fragments differ only little for D_2O and H_2O. More specifically,

for excitation in the peak of the absorption band, the average vibrational energy in the OX fragment is 0.45 eV for OD and 0.55 eV for OH.[15] Correcting Eq. (3) for the vibrational energy loss to the OX fragment (by subtracting these numbers from ΔE, where ΔE can be taken equal to 3.2 eV (see Arasa *et al.*[12] and Ref. 53 therein)) leads to little change in the ratio E_{OD}/E_{OH} predicted by Eq. (3); if anything, the ratio should become a little bit larger. Applying this correction, Eq. (3) predicts that on average OD is released from D_2O with an initial kinetic energy of 0.275 eV, while OH should be released from H_2O with an initial kinetic energy of 0.147 eV. Furthermore, we note that although in an ice surface the excited molecule is not isolated but interacts with other water molecules during the MD calculations, the energy and momentum conservation laws can still be used to have an approximation of the initial kinetic energy of the photofragments.

(2) It is likely that the hyperthermal OX formed following photodissociation will lose its energy most easily to phonons of the surrounding ice lattice with frequencies close to its translational energy. These phonons are the librations. In H_2O, the librations have considerably higher frequencies than in D_2O, the highest observed frequency being 110 meV for H_2O and 84 meV for D_2O.[44] For this reason, we suspect that the energetic OX will lose its energy more easily to the H_2O lattice than to the softer D_2O lattice. The initially formed OD radical has greater initial energy (e.g., at 10 K, the averaged kinetic energy taken over the top four MLs is 0.263 eV, compared to 0.275 eV predicted from Eq. (3) and considering vibrational excitation of the OD fragment, see above), and OH less initial energy (e.g., at 10 K, the averaged kinetic energy taken over the top four MLs is 0.200 eV, compared to a predicted value of 0.147 eV). However, the hyperthermal OD fragment formed will transfer its energy more easily to the H_2O lattice, which has higher frequency librations (up to 110 meV[44]), than OH will transfer its energy to the softer D_2O lattice, which has lower frequency vibrations (up to 84 meV[44]). We speculate that these opposing trends explain why the photodesorption probabilities of OD from an H_2O ice system and OH from a D_2O ice system are similar. Higher initial energies of the OD radical upon D_2O dissociation than the OH radical upon H_2O dissociation and more efficient energy transfer from the OX radical to the H_2O ice than to the D_2O ice explain the trends observed in Fig. 3. The comparison also suggests that the OX photodesorption probability is predominantly determined by the initial kinetic energy: averaged over T_{ice}, the probability of the more energetic OD to desorb from H_2O ice is somewhat larger than that of OH to desorb from D_2O ice, even though energy should be more easily transferred to the harder H_2O lattice.

C. X_2O molecule photodesorption

The third photodesorption channel is X_2O molecule photodesorption, which can occur through the direct desorption of the recombined X_2O molecule or through the kick-out mechanism.[6,7]

In Fig. 4 the direct photodesorption probabilities of recombined X_2O averaged over the top four MLs are plotted versus the ice temperature for the first four dissociation scenarios listed in Sec. II C, using the same scale as for the other X_2O photodesorption mechanism in Fig. 5. For direct X_2O desorption, no isotope effects are observed. If recombination of the fragments does occur in the top MLs, the produced molecule is highly energetic, and the recombined X_2O molecule can still desorb. However, if the dissociation occurs deeper in the ice, the newly formed water molecule loses its energy upon collisions with other water molecules and the desorption of the recombined X_2O molecule becomes unlikely due to strong interaction with the other water molecules. The fact that no isotope effects are observed in the direct photodesorption of X_2O molecules suggests that in this mechanism the desorption probability is determined by the available excess energy upon recombination, which is very similar for H_2O and D_2O ice, which have very similar absorption spectra.

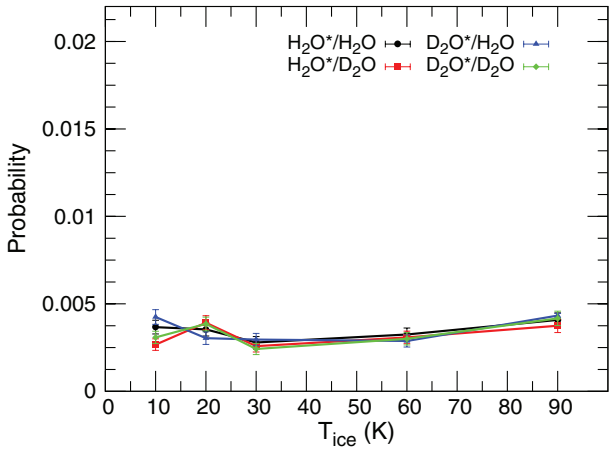

FIG. 4. Photodesorption probabilities of recombined X_2O molecules following X_2O photodissociation in an X_2O ice system (denoted as X_2O X_2O^*/X_2O) averaged over the top four MLs as a function of T_{ice}.

On the other hand, isotope effects are rather noticeable if X_2O desorbs from the ice surface through the kick-out mechanism (Fig. 5). The kick-out mechanism is more likely to happen if D_2O is initially excited. This can be explained by

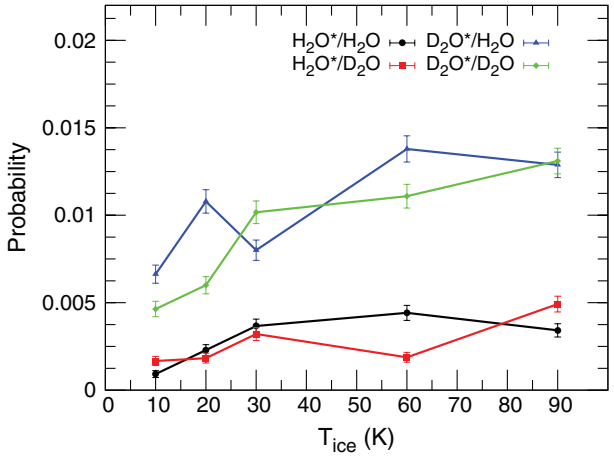

FIG. 5. Photodesorption probabilities of the X_2O molecules via the kick-out mechanism following X_2O photodissociation in an X_2O ice system (denoted as X_2O X_2O^*/X_2O) averaged over the top four MLs as a function of T_{ice}.

TABLE II. Mass ratios (α) and energy transfer efficiencies (r) for collisions between an X atom and a stationary X_2O molecule (X/X_2O).

X/X_2O	α	r
H/H_2O	0.056	0.20
H/D_2O	0.050	0.18
D/H_2O	0.111	0.36
D/D_2O	0.100	0.33

the efficiency of the energy transfer in a collision of an X atom with an X_2O molecule in the ice surface. The mass ratio between D and X_2O is higher than the mass ratio between H and X_2O, and therefore D can transfer its energy more easily upon a collision with an X_2O molecule. The mass ratios and the values of the fraction of energy transferred (Eq. (2)) for each kick-out scenario are summarized in Table II.

The kick-out mechanism is more likely to occur if the molecule that is initially excited and that neighbours the X_2O molecule to be desorbed is a D_2O molecule. (The condition that these molecules need to be close to each other is due to the high binding energy of X_2O molecules to the surface ≈0.3 eV and the unfavorable mass ratio between even D-atoms and X_2O: D- or H-atoms that have already lost part of their kinetic energy through encounters with other X_2O molecules will not be able to kick-out a surface X_2O molecule.) This can be explained by the efficiency of the energy transfer in a collision of a hydrogen atom of unknown mass, but with high initial kinetic energy, to an X_2O molecule in one of the topmost layers. The mass ratio between D and X_2O is higher than the mass ratio between H and X_2O, and therefore an energetic D atom can transfer its energy more efficiently to the neighbouring X_2O molecule and cause it to desorb than an H atom with the same energy (Table II).

A temperature effect on the photodesorption probabilities can be observed in Fig. 5, as the kick-out probability rises with ice temperature (e.g., the average kick-out probabilities at 10 K are 0.13% and 0.56% if an H_2O molecule or a D_2O molecule is initially dissociated, respectively, and the average kick-out probabilities at 90 K are 0.42% and 1.30% if an H_2O molecule or a D_2O molecule is initially dissociated, respectively). We attribute the higher desorption probability to the higher kinetic energy the desorbing molecules may already have at higher ice temperatures prior to receiving a kick from the X photofragment.

In Fig. 6 the total X_2O desorption probabilities are plotted, which are sums of the direct photodesorption probabilities and the kick-out probabilities. The total X_2O photodesorption probabilities are largest for D_2O^* because the kick-out mechanism is most efficient for D_2O^*, and the direct mechanism displays no isotope effects.

The photodesorption probabilities of oxygen containing species following X_2O^* photodissociation in X_2O ice ($Y_{X_2O^*/X_2O}$) can be calculated as the sum of the probabilities from Figs. 3 and 6, and summarized as follows:

$$Y_{D_2O^*/D_2O} > Y_{D_2O^*/H_2O} > Y_{H_2O^*/D_2O} > Y_{H_2O^*/H_2O}.$$

The photodesorption of an oxygen containing species is most probable if D_2O is dissociated in a D_2O ice system, because of the large photodesorption probabilities of OD radicals from D_2O ice. The photodesorption probabilities of OH radicals from a D_2O ice system are similar to those for OD radicals from an H_2O ice system, however the kick-out probabilities are larger if D_2O is initially dissociated than if H_2O is initially dissociated. The photodesorption of an oxygen containing species is least probable if H_2O is dissociated in a H_2O ice system, because of the lower OH radical desorption probabilities and the lower kick-out probabilities if H_2O is initially dissociated than if D_2O is dissociated.

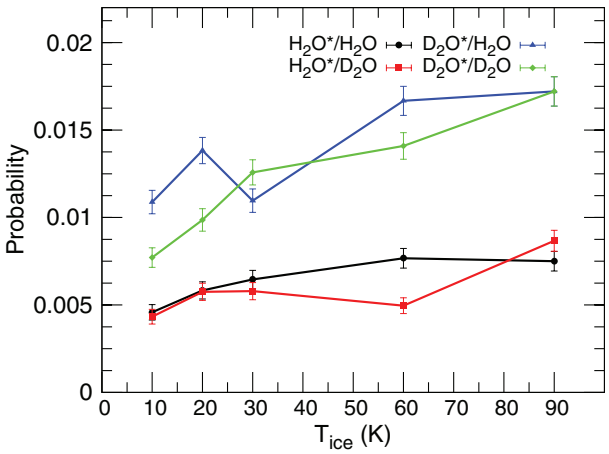

FIG. 6. Photodesorption probabilities of X_2O molecules via either mechanism (direct desorption of recombined X_2O molecules and kick-out of X_2O molecules) from an X_2O ice system averaged over the top four MLs as a function of T_{ice}, the legend denotes the photo-excited molecule and the ice system (X_2O^*/X_2O).

D. HOD photodesorption processes

Photodissociation of an HOD molecule can lead to two sets of products: D + OH and H + OD. The photodesorption processes of the HOD molecule are considered individually for both sets of dissociation products. The absorption spectra based on the Wigner distributions for the "HOD" and the "DOH" (see also Sec. II C) molecule in H_2O ice at 10 K are shown in Fig. 7(b) for HOD molecules located in the top 5 MLs. In principle, the absorption spectrum of HOD should not depend on the choice of the Jacobi coordinates of the HOD molecule. However, since the total wavefunction of the vibrational ground state is approximated by a product of uncoupled wavefunctions (Eq. (5.19) in Ref. 35), the motions of the OD and the OH vibrations are no longer coupled and the absorption spectra of HOD and DOH may differ slightly. The absorption spectrum of H_2O ice is blueshifted by 1 eV[6,45] relative to the absorption spectrum of gas-phase H_2O. A similar blueshift is expected for the absorption spectrum of HOD in H_2O ice. The maxima of the absorption spectra are 8.59 and 8.54 eV for the "HOD" and the "DOH" molecule, respectively. These results are then consistent with the maximum at 7.45 eV of the gas-phase HOD absorption spectrum computed by Van Harrevelt *et al.*[15] (Fig. 7(a)) and the blueshift noted. The computed absorption spectra for HOD in ice (Fig. 7(b)) have a tail at the low-energy end of the spectrum, whereas the gas-phase HOD absorption spectrum (Fig. 7(a)) has a

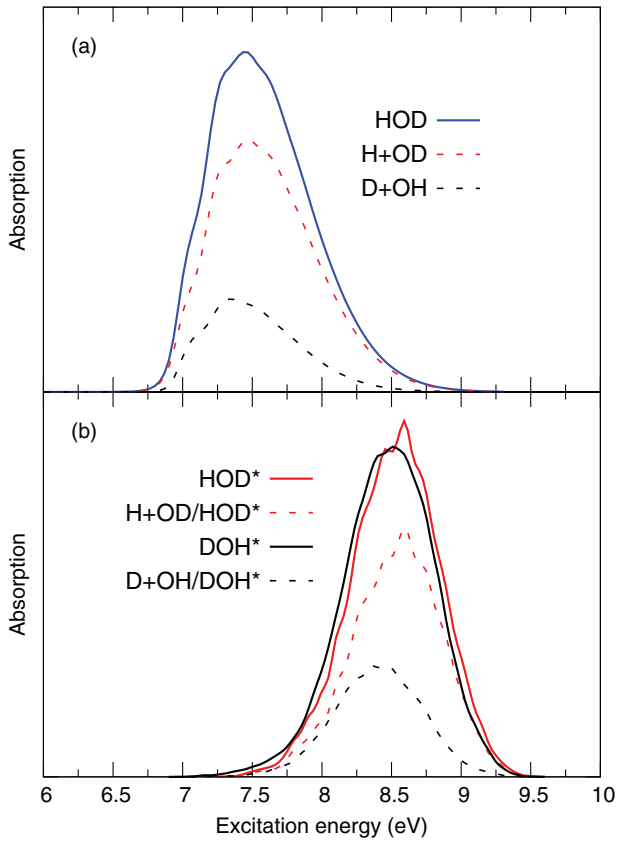

FIG. 7. (a) Gas-phase absorption spectrum for the HOD molecule (blue line), which is the sum of the H + OD (red dashed line) and the D + OH (black dashed line) partial spectra. Data obtained from Ref. 46. (b) The absorption spectra for the HOD molecule using the Wigner distributions specifically made for the HOD →H + OD dissociation reaction (red solid line, HOD* in the legend) and for the HOD →D + OH dissociation reaction (black solid line, DOH* in the legend) at T_{ice}=10 K. The dashed lines represent the absorption associated with the trajectories that lead to desired dissociation events in the top four MLs, H + OD (red dashed line) or D + OH (black dashed line). Spectra were made by binning the excitation energies into 0.05 eV-wide energy intervals.

tail at the high-energy end of the spectrum. The tail at the low-energy end of the absorption spectrum of HOD in ice is caused by excitation of HOD molecules in the first ML. These molecules have no other water molecules above them, therefore they resemble a gas-phase HOD molecule more closely than HOD molecules located in MLs 2–5. The blueshift in photon-absorption energy from gas-phase HOD to HOD in ice is therefore less pronounced for the HOD molecule in the first ML, thus introducing a tail at the low-energy end of the absorption spectrum. The partial absorption spectra of the trajectories that lead to photofragments H + OD and the ones that lead to D + OH for HOD in the gas-phase and in the ice display similar features.

To estimate the initial kinetic energies of the photofragments upon dissociation, we use the momentum and energy conservation laws described in Sec. III B. The initial energies of the $OX^{(2)}$ photofragments corresponding to $X^{(1)}OX^{(2)} \rightarrow OX^{(2)} + X^{(1)}$ are computed using Eq. (3) for $X^{(1)}$ = H or D and $X^{(2)}$ = H or D. The estimated energies of the photofragments are summarized in Table III.

TABLE III. Estimated initial kinetic energies of the photofragments as a fraction of the energy available upon photodissociation of $X^{(1)}OX^{(2)}$ in a vacuum, according to Eq. (3).

Scenario in H_2O ice	Dissociation reaction	Fractional energy photofragment $OX^{(2)}$	Fractional energy photofragment $X^{(1)}$
1	$H_2O \rightarrow H + OH$	0.056	0.94
5	$HOD \rightarrow H + OD$	0.053	0.95
6	$HOD \rightarrow D + OH$	0.11	0.89
3	$D_2O \rightarrow D + OD$	0.10	0.90

In this section photodesorption probabilities are provided given that a specific dissociation reaction has occurred, rather than that a specific photo-excitation event has occurred (e.g., OH desorption probabilities given the HOD → D + OH reaction, rather than OH desorption probabilities given excitation of the HOD molecule). This issue did not exist in the previous sections because X_2O only has one dissociation reaction: $X_2O \rightarrow X + OX$. The $OX^{(2)}$ radical photodesorption probabilities defined in this way and averaged over the top four MLs are plotted in Fig. 8 for dissociation scenarios 1, 3, 5, and 6. On a relative basis the photodesorption probabilities of the OH radical formed upon HOD photodissociation and the OD radical formed upon D_2O photodissociation are much higher than those of the OD radical formed upon HOD photodissociation or the OH radical formed upon H_2O photodissociation. This observation can be explained by the initial kinetic energies of the $OX^{(2)}$ radicals (see Table III). The energy of the $OX^{(2)}$ radical resulting from dissociated $DOX^{(2)}$ is about twice the energy of the $OX^{(2)}$ if the dissociated molecule is $HOX^{(2)}$. Therefore, on a relative scale, the photodesorption of the OX radical is much more likely if the dissociated molecule is $DOX^{(2)}$ than if it is $HOX^{(2)}$.

The MD simulations suggest that the isotope fractionation of OX through photodissociation of water in the ISM is influenced by photodesorption processes. Averaged over T_{ice}, following initial dissociation of HOD into D + OH the OH radical is a factor 2.14 more likely to desorb from the ice surface than the OD radical following initial dissociation of

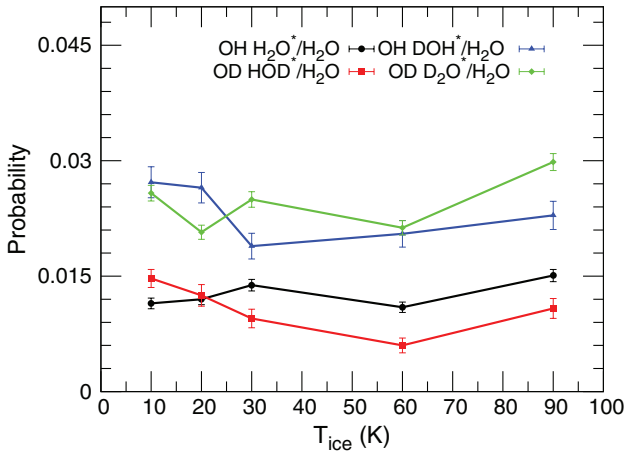

FIG. 8. Photodesorption probability of the $OX^{(2)}$ radical following $X^{(1)}OX^{(2)}$ photodissociation in an H_2O ice system (denoted in the legend as OX $X^{(1)}OX^{(2)}$*/H_2O) averaged over the top four MLs versus ice temperature T_{ice}.

TABLE IV. $\frac{OD}{OH}$ ratios following: HOD dissociation in the gas-phase, HOD dissociation in ice, and photodesorption of OX radicals given HOD excitation in ice. Reaction branching ratios are computed by integrating the partial absorption spectra over the complete energy range of the first absorption band. The $\frac{OD_{des}}{OH_{des}}$ ratio is obtained using Eq. (4).

HOD photodissociation	Temperature (K)	$\frac{OD}{OH}$ ratio
Gas-phase HOD		3.1[46]
HOD in H_2O ice	10	2.20
	20	2.25
	30	2.25
	60	2.27
	90	2.26
Photodesorption ($\frac{OD_{des}}{OH_{des}}$)	10	1.20
	20	1.08
	30	1.16
	60	0.67
	90	1.08

HOD into H + OD (Fig. 8). Also, the branching ratio $\frac{H+OD}{D+OH}$ of the HOD photodissociation reaction, which can be computed by integrating the H + OD and the D + OH partial absorption spectra, for HOD in ice is 2.20 at $T_{ice} = 10$ K (see Fig. 7(b)). HOD photodissociation branching ratios ($\frac{H+OD}{D+OH}$) have been computed for each ice temperature and are summarized in Table IV. Also, the photodesorption ratios ($\frac{OD_{des}}{OH_{des}}$) following the HOD photodissociation reaction have been calculated using

$$\frac{OD_{des}}{OH_{des}}(T_{ice}) = \frac{\sum_{i=1}^{4} P_{OD_{des}}(i, T_{ice}) \frac{\beta(i,T_{ice})}{1+\beta(i,T_{ice})}}{\sum_{i=1}^{4} P_{OH_{des}}(i, T_{ice}) \frac{1}{1+\beta(i,T_{ice})}} \quad (4)$$

where $P_{OD_{des}}(i, T)$ is the OD photodesorption probability given the HOD dissociation reaction into H + OD in ML i at $T = T_{ice}$, $P_{OH_{des}}(i, T)$ is the OH photodesorption probability given the HOD dissociation reaction into D + OH in ML i at $T = T_{ice}$, and $\beta(i, T)$ is the HOD photodissociation branching ratio $\frac{H+OD}{D+OH}$ in ML i at $T = T_{ice}$. All $\frac{OD_{des}}{OH_{des}}$ ratios are also summarized in Table IV. On average, the HOD photodissociation reaction branching ratio in water ice is ~2.2 and the photodesorption branching ratio following HOD photodissociation is equal to 1.0, with a standard deviation of 0.2. (To compute the latter two quantities, we have assumed the photodesorption branching ratio to be independent of T_{ice}, i.e., we have assumed that the differences in the values for this quantity in Table IV reflect statistical uncertainties.)

One reason that the photodesorption ratio OD/OH computed here (1.0) is lower than the gas phase OH/OD photodissociation ratio (3.1, Table IV) is that in the ice surface the initial OH/OD photodissociation ratio (2.25 ± 0.01, Table IV) is much lower than the gas phase value (3.1). We attribute the lower value of the OH/OD photodissociation ratio in ice at least in part to caging effects. An important reason for the large ratio in gas phase photodissociation is kinematic:[43] in response to the repulsive forces experienced on the excited state intramolecular potential, the lighter H-atom is able to move faster towards the exit channel. However, in an ice matrix, much of the kinematic advantage the H-atom has over the D-atom may disappear due to caging effects: there may be trajectories in which the HDO molecule first recombines because the released atom rebounds from a surrounding water molecule. Here, the lighter H-atom would be at a disadvantage, i.e., it would be more likely to rebound and temporarily reform HOD than the heavier D-atom. The fact that we compute a larger average value (averaged over T_{ice}) for $\beta(1)$ (2.31 ± 0.02) than for $\beta(4)$ (2.22 ± 0.01) supports this argument, as caging should be less important in the topmost layer of the ice surface than in the bulk of the ice. However, electronic effects of the surrounding water molecules can also be important, as the presence of even one additional water molecule can lead to considerable changes in the shape of the potential energy surface of the excited water molecule.[47] Because OH photodesorption probabilities following HOD photodissociation are higher than those for OD, gaseous OH formation is favored if HOD photodissociation occurs in ice rather than in the gas-phase. The $\frac{OD}{OH}$ ratio in the gas-phase is therefore expected to be lower in dense clouds, where photodesorption of OX radicals from the ice may additionally affect this ratio, than in diffuse clouds where OX radical photodesorption from ice does not occur.

No isotope effects are observed on the photodesorption probabilities of recombined HOD molecules, as is the case for the photodesorption probabilities of recombined X_2O molecules. The kick-out of surrounding H_2O molecules (Fig. 9) does show isotope effects. The kick-out mechanism is more likely to occur if the D photofragment is formed, because the D atom transfers its momentum to the water molecules upon collisions more easily than the H atom does.

It can also be observed that, in most cases, the kick-out probability of an H_2O molecule is slightly higher if the D atom is formed upon photodissociation of D_2O than upon photodissociation of HOD. (We attribute the observation of the reverse order in magnitude at $T_{ice} = 90$ K to statistical uncertainties in the calculations, as reflected in the overlapping error bars for this surface temperature). This observation can be explained from the initial kinetic energy of the D atom. The maximum of the partial absorption spectrum of the trajectories that lead to D + OH lies at 8.4 eV, whereas the maximum is at 8.6 eV for the D_2O absorption spectrum.

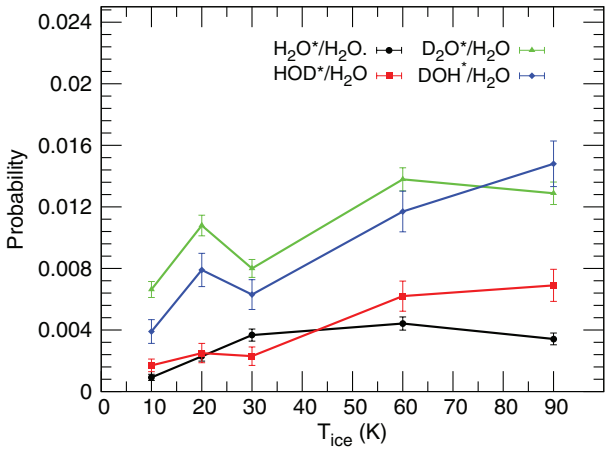

FIG. 9. Photodesorption probabilities of H_2O molecules due to the kick-out mechanism subsequent to $X^{(1)}OX^{(2)}*$ photodissociation in H_2O ice (denoted in the legend as $X^{(1)}OX^{(2)}*/H_2O$) averaged over the top four MLs versus T_{ice}.

This can be explained by the zero-point energy of the OD vibration being lower than that of the OH vibration. Therefore, a larger fraction of the available energy can go to the D atom upon D_2O photodissociation than upon HOD photodissociation. Also, the estimated fraction of the available energy which goes to the D atom upon HOD photodissociation into D + OH is $0.895E$, whereas the energy of the D atom upon D_2O photodissociation is $0.900E$ (see Table III). This means that based on the mass ratio of the photofragments, on average, the D atom will receive 0.016 eV less energy if an HOD molecule is dissociated than if a D_2O molecule is dissociated, taking $E_{diss} \approx 5.4$ eV.[15] These considerations indicate that the D atom initially receives less energy upon dissociation of HOD than upon dissociation of D_2O, which explains the lower kick-out probabilities if the D atom is created upon photodissociation of HOD instead of D_2O.

The $X^{(1)}$ atom photodesorption probabilities averaged over the top four MLs for dissociation scenarios 1, 3, 5, and 6 listed in Sec. II C are plotted versus T_{ice} in Fig. 10. The H atom photodesorption probability is larger than the D atom photodesorption probability. The averaged H atom photodesorption probability following HOD or H_2O dissociation in H_2O amorphous ice over all T_{ice} is 58.5% and 58.8%, respectively, whereas the averaged D atom photodesorption probability following HOD or D_2O dissociation in H_2O amorphous ice is 54.0% and 55.3%, respectively. The H atom desorption probabilities are very similar upon HOD and H_2O dissociation, however the D atom photodesorption probability is in each case slightly lower if HOD is dissociated than if D_2O is dissociated. This might be a manifestation of the somewhat lower initial kinetic energy that the D atom receives upon HOD dissociation than upon D_2O dissociation.

The difference in H atom and D atom photodesorption probabilities can be explained by the mass ratio between the $X^{(1)}$ atom and the water molecules (Sec. III A). The mass ratio between the D atom and the H_2O ice is higher than the mass ratio between the H atom and the H_2O ice, which means that the energy transfer from the D atom to the ice is more efficient than from the H atom to the ice. As a result, the D atom loses more energy to the ice leading to a lower D atom photodesorption probability relative to the H atom.

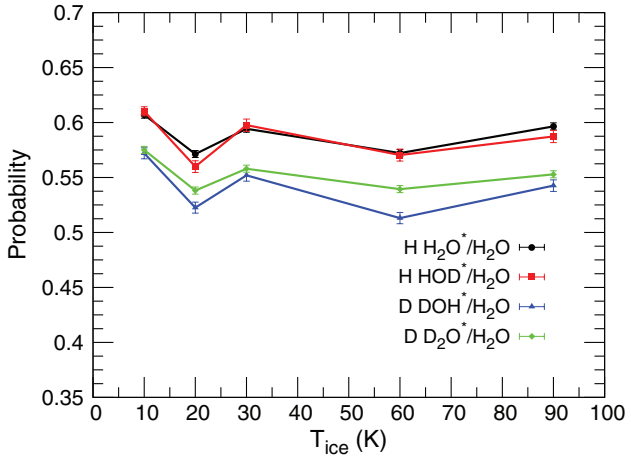

FIG. 10. Photodesorption probabilities of photofragment $X^{(1)}$ upon dissociation of $X^{(1)}OX^{(2)}*$ in H_2O ice (denoted in the legend as X $X^{(1)}OX^{(2)}*/H_2O$) averaged over the top four MLs as a function of ice temperatures (T_{ice}).

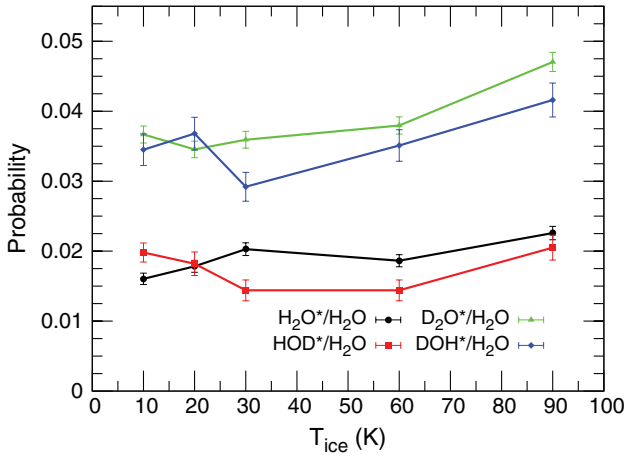

FIG. 11. Photodesorption probability of all oxygen containing species (OX radical, recombined $X^{(1)}OX^{(2)}$ molecule and H_2O molecule) following $X^{(1)}OX^{(2)}*$ photodissociation in H_2O ice (denoted $X^{(1)}OX^{(2)}*/H_2O$ in the legend) averaged over the top four MLs plotted versus T_{ice}.

The photodesorption probability of oxygen containing species is most probable if the D atom is formed upon dissociation of the $X^{(1)}OX^{(2)}$ molecule, as can be seen in Fig. 11. The initial kinetic energy of the $OX^{(2)}$ radical is larger if the $X^{(1)}$ atom is D, which leads to higher OX desorption probabilities. Also, the D atom transfers momentum more easily to a surrounding H_2O molecule than an H atom does, leading to higher kick-out photodesorption probabilities.

IV. CONCLUSIONS

In this work we have carried out MD calculations on photodissociation of X_2O (X = H,D) molecules in X_2O (X = H,D) amorphous ice and HOD molecules in H_2O amorphous ice after UV photon excitation to the first electronically excited state in order to investigate the isotope effects on the associated photodesorption processes. Isotope effects are observed for X atom photodesorption, OX radical photodesorption, and also for the X_2O molecule photodesorption through the kick-out mechanism, whereas no isotope effects are observed for the direct photodesorption process of the recombined X_2O or HOD molecule.

The OX radical photodesorption probability is larger if a DOX molecule is dissociated than if an HOX molecule is dissociated. If an HOD molecule is dissociated into D + OH, the OH radical photofragment is, averaged over the top four MLs and all ice temperatures, about a factor 1.8 more likely to desorb from an H_2O ice system than the OH radical formed upon dissociation of an H_2O, whereas if an HOD molecule is dissociated into H + OD, the OD is about a factor 2.3 less likely to desorb from an H_2O ice surface than the OD radical formed upon D_2O photodissociation. This is the case because the initial kinetic energy of the OX radical is much larger (about a factor 1.9) if the dissociating molecule is DOX than if it is HOX. Also, the OX radical photodesorption probability is larger if the ice system is D_2O. This observation can be explained by more efficient energy transfer from the OX radicals

to the H_2O ice system, which has higher libration frequencies, than to the D_2O ice system.

Averaged over T_{ice}, the OH radical photodesorption probability following HOD dissociation into D + OH is about a factor 2.14 larger than the OD radical photodesorption probability following HOD photodissociation into H + OD. Also, the branching ratio of the HOD photodissociation reaction $\frac{H+OD}{D+OH}$ in the ice is ∼2.2, which is lower than that for the gas-phase HOD photodissociation reaction, which is estimated to be ∼3.1. Thus, relative to gas-phase photodissociation of HOD, the gaseous OH radical becomes more likely to be formed and the gaseous OD radical becomes less likely to be formed if the photodissociation event occurred in the ice. These observations suggest that the $\frac{OD(g)}{OH(g)}$ ratio in the ISM could be different for dense and diffuse clouds, as ice should be present in the former, but not in the latter.

The kick-out mechanism, by which an X_2O molecule desorbs from the surface through a kick of an energetic X atom, is more likely to occur if D atoms are formed through D_2O or HOD photodissociation than if H atoms are formed upon H_2O or HOD photodissociation, since D atoms can transfer their energy more easily to X_2O molecules in the ice than H atoms can. Whether the ice is made from H_2O or D_2O molecules does not influence the kick-out probabilities greatly. However, the kick-out probability does rise with increasing ice temperatures, which we attribute to the water molecules having more kinetic energy at higher ice temperature and thus needing less energy to be transferred from the X photofragment upon a collision to be able to desorb.

The X atom photodesorption probability is larger if the H atom is formed upon HOD or H_2O photodissociation than if a D atom is formed upon HOD or D_2O photodissociation. H atoms desorb more easily from the surface than D atoms, because H atoms have higher initial kinetic energies than D atoms. Moreover, D atoms transfer their energies more easily to the surrounding water molecules than H atoms do. The D atom photodesorption probability averaged over all the considered ice temperatures following dissociation of the excited molecule in one of the top four MLs is about a factor 0.9 times the H atom photodesorption probability.

ACKNOWLEDGMENTS

The authors would like to thank M. C. van Hemert for discussions on the setup of the Wigner distributions and the data for the gas-phase partial absorption spectra of HOD, and S. Andersson for providing the initial MD photodissociation code. This project was funded by NWO astrochemistry Grant No. 648.000.010.

[1]E. L. Gibb, D. C. B. Whittet, W. A. Schutte, A. C. A. Boogert, J. E. Chiar, P. Ehrenfreund, P. A. Gerakines, J. V. Keane, A. G. G. M. Tielens, E. F. van Dishoeck, and O. Kerkhof, Astrophys. J. **536**, 347 (2000).
[2]A. C. A. Boogert, K. M. Pontoppidan, C. Knez, F. Lahuis, J. Kessler-Silacci, E. F. van Dishoeck, G. A. Blake, J.-C. Augereau, S. E. Bisschop, S. Bottinelli, T. Y. Brooke, J. Brown, A. Crapsi, N. J. Evans II, H. J. Fraser, V. Geers, T. L. Huard, J. K. Jørgensen, K. I. Öberg, L. E. Allen, P. M. Harvey, D. W. Koerner, L. G. Mundy, D. L. Padgett, A. I. Sargent, and K. R. Stapelfeldt, Astrophys. J. **678**, 985 (2008).
[3]K. I. Öberg, H. Linnartz, R. Visser, and E. F. van Dishoeck, Astrophys. J. **693**, 1209 (2009).
[4]E. A. Bergin, W. D. Langer, and P. F. Goldsmith, Astrophys. J. **441**, 222 (1995).
[5]H. J. Fraser, M. P. Collings, M. R. S. McCoustra, and D. A. Williams, Mon. Not. R. Astron. Soc. **327**, 1165 (2001).
[6]S. Andersson, A. Al-Halabi, G. J. Kroes, and E. F. van Dishoeck, J. Chem. Phys. **124**, 064715 (2006).
[7]S. Andersson and E. F. van Dishoeck, Astron. Astrophys. **491**, 907 (2008).
[8]T. Hama, M. Yokoyama, A. Yabushita, M. Kawasaki, S. Andersson, C. M. Western, M. N. R. Ashfold, R. N. Dixon, and N. Watanabe, J. Chem. Phys. **132**, 164508 (2010).
[9]E. Herbst and E. F. van Dishoeck, Annu. Rev. Astron. Astrophys. **47**, 427 (2009).
[10]R. T. Garrod and E. Herbst, Astron. Astrophys. **457**, 927 (2006).
[11]R. T. Garrod, S. L. Widicus Weaver, and E. Herbst, Astrophys. J. **682**, 283 (2008).
[12]C. Arasa, S. Andersson, H. M. Cuppen, E. F. van Dishoeck, and G. J. Kroes, J. Chem. Phys. **134**, 164503 (2011).
[13]V. Engel and R. Schinke, J. Chem. Phys. **88**, 6831 (1988).
[14]V. Engel, R. Schinke, and V. Staemmler, J. Chem. Phys. **88**, 129 (1988).
[15]R. van Harrevelt and M. C. van Hemert, J. Chem. Phys. **114**, 9453 (2001).
[16]J. Zhang, D. G. Imre, and J. H. Frederick, J. Phys. Chem. **93**, 1840 (1989).
[17]X. F. Yang, D. W. Hwang, J. J. Lin, and X. Ying, J. Chem. Phys. **113**, 10597 (2000).
[18]B. M. Cheng, E. P. Chew, C. P. Liu, M. Bahou, Y. P. Lee, Y. L. Yung, and M. F. Gerstell, Geophys. Res. Lett. **26**, 3657, doi:10.1029/1999GL008367 (1999).
[19]H. t. Wang, W. S. Felps, and S. P. McGlynn, J. Chem. Phys. **67**, 2614 (1977).
[20]K. Yoshino, J. R. Esmond, W. H. Parkinson, K. Ito, and T. Matsui, Chem. Phys. **211**, 387 (1996).
[21]K. Weide, S. Henning, and R. Schinke, J. Chem. Phys. **91**, 7630 (1989).
[22]M. Sarma, S. Adhikari, and M. K. Mishra, J. Chem. Sci. **119**, 377 (2007).
[23]S. Legendre, E. Giglio, M. Tarisien, A. Cassimi, B. Gervais, and L. Adoui, J. Phys. B: At. Mol. Opt. Phys. **38**, L233 (2005).
[24]R. L. Vander Wal, J. L. Scott, F. F. Crim, K. Weide, and R. Schinke, J. Chem. Phys. **94**, 3548 (1991).
[25]S. Andersson, G. J. Kroes, and E. F. van Dishoeck, Chem. Phys. Lett. **408**, 415 (2005).
[26]C. Arasa, S. Andersson, H. M. Cuppen, E. F. van Dishoeck, and G. J. Kroes, J. Chem. Phys. **132**, 184510 (2010).
[27]M. S. Westley, R. A. Baragiola, R. E. Johnson, and G. A. Baratta, Planet. Space Sci. **43**, 1311 (1995).
[28]M. S. Westley, R. A. Baragiola, R. E. Johnson, and G. A. Baratta, Nature (London) **373**, 405 (1995).
[29]A. Yabushita, T. Hama, M. Yokoyama, M. Kawasaki, S. Andersson, R. N. Dixon, M. N. R. Ashfold, and N. Watanabe, Astrophys. J. **699**, L80 (2009).
[30]P. M. Hundt, R. Bisson, and R. D. Beck, J. Chem. Phys. **137**, 074701 (2012).
[31]E. R. Batista, P. Ayotte, A. Bilić, B. D. Kay, and H. Jónsson, Phys. Rev. Lett. **95**, 223201 (2005).
[32]W. L. Jorgensen, J. Chandrasekhar, J. D. Madura, R. W. Impey, and M. L. Klein, J. Chem. Phys. **79**, 926 (1983).
[33]A. J. Dobbyn and P. J. Knowles, Mol. Phys. **91**, 1107 (1997).
[34]F. J. Aoiz, L. Bañares, J. F. Castillo, M. Brouard, W. Denzer, C. Vallance, P. Honvault, J.-M. Launay, A. J. Dobbyn, and P. J. Knowles, Phys. Rev. Lett. **86**, 1729 (2001).
[35]R. Schinke, *Photodissociation Dynamics* (Cambridge University Press, Cambridge, 1993).
[36]T. Shimanouchi, *Tables of Molecular Vibrational Frequencies. Consolidated Volume I*, National Standard Reference Data Series 39 (NSRDS-NBS 39) (National Bureau of Standards; U.S. Govt. Print. Off., US, 1972).
[37]W. S. Benedict, N. Gailar, and E. K. Plyler, J. Chem. Phys. **24**, 1139 (1956).
[38]N. M. Gailar and F. P. Dickey, J. Mol. Spectrosc. **4**, 1 (1960).
[39]A. Amirav, M. J. Cardillo, P. L. Trevor, C. Lim, and J. C. Tully, J. Chem. Phys. **87**, 1796 (1987).
[40]A. Al-Halabi, A. W. Kleyn, and G. J. Kroes, J. Chem. Phys **115**, 482 (2001).

[41]A. Al-Halabi, A. W. Kleyn, E. F. van Dishoeck, and G. J. Kroes, J. Phys. Chem. B **106**, 6515 (2002).
[42]L. Amiaud, F. Dulieu, J.-H. Fillion, A. Momeni, and J. L. Lemaire, J. Chem. Phys. **127**, 144709 (2007).
[43]V. Engel, V. Staemmler, R. L. Vander Wal, F. F. Crim, R. J. Sension, B. Hudson, P. Andresen, S. Hennig, K. Weide, and R. Schinke, J. Phys. Chem. **96**, 3201 (1992).
[44]P. Bosi, R. Tubino, and G. Zerbi, J. Chem. Phys. **59**, 4578 (1973).
[45]K. Kobayashi, J. Phys. Chem. **87**, 4317 (1983).
[46]R. van Harrevelt and M. C. van Hemert, private communication (2012) regarding unpublished data in Table I in Ref. 15.
[47]G. Avila, G. J. Kroes, and M. C. van Hemert, J. Chem. Phys. **128**, 144313 (2008).